Supporting Information

Tovar-Moll et al. 10.1073/pnas.1400806111

Neuropsychological Testing

Besides the tests aiming specifically at probing tactile interhemispheric transfer, background neuropsychological tests were used in all callosal dysgenesis (CD) subjects (Table S1) and controls for: (*i*) praxis and writing; (*ii*) daily functional capacity (1); (*iii*) severe impairment of memory (immediate and delayed recall), language (comprehension and production), motor performance, conceptualization, and general knowledge (1); (*iv*) handedness (2, 3); and (*v*) general intelligence, IQ (4, 5). A summary of the results are provided in Table S2.

Praxis and Writing. Ideomotor praxis was evaluated by asking subjects to pantomime the following gestures: brush the teeth, comb the hair, and wave good-bye. Basic writing skills were assessed by asking participants to write down their own names. These tasks were tested first with the left and then with the right hand to avoid left to right cross cueing between the hemispheres.

Barthel Index. The Barthel Index (BI) (6) assesses the fundamental aspects of functional capacity: that is, the degree of independence in carrying out basic activities of daily living. These activities are related to personal care and survival as gauged by the following items: feeding, personal care (bathing and grooming), dressing, bowel and bladder control, and mobility. Total BI scores range from zero (full dependence) to 100 (full independence).

Test for Severe Impairment. The Test for Severe Impairment (TSI) (1) assesses the following cognitive domains: memory (immediate and after a short delay), language (comprehension and production), motor performance, conceptualization, and general knowledge. The TSI is administered in ∼10 min and has the additional advantage of requiring spoken language skills on only eight out of its 24 items; the remaining 16 items depend on the examinee's performance, which is mainly comprised of meaningful gestures and the manipulation of familiar objects (comb, pen) to accomplish certain ends. TSI scores range from 0 (worst performance) to 24 (best performance).

Edinburgh Handedness Inventory. Handedness was assessed with the Brazilian validated version of the Edinburgh Handedness Inventory (EHI) (2, 3). The form used in this study included 10 items, the laterality quotient ranging from –100 (fully left-handed) to +100 (fully right-handed).

Intelligence Quotient. The intelligence quotient (IQ) was estimated using the Vocabulary and Block Design subtests of the Wechsler Intelligence Scale for Children and Adults (4, 5). The combination of the Vocabulary and Block Design subtests has a high correlation with the Full Scale IQ ($r > 0.90$) and stands out as one of the best predictors of the full scale IQ (7, 8).

Statistical Analyses. The degree of association between nominal variables (9) was assessed with χ^2 tests. The significance of differences between averages for controls and CD was assessed with the Mann–Whitney *U* test, and the significance of the differences between intragroup pairs of variables was assessed with the Wilcoxon test (10). The strength of the association between dimensional variables was ascertained with Spearman correlation coefficient (ρ). Unless stated otherwise, a significance threshold (α) of 0.05 was adopted for all statistical tests. The size effects and power of the statistical tests were computed with G*Power v. 3.1 following the guidelines of Cohen (11).

Image Acquisition and Processing

Functional Resting-State Functional MRI. Probabilistic independent component analysis (ICA) was used to decompose the resting-state functional MRI (rs-fMRI) time courses data into different temporal and spatial components, according to the standard FEAT (FMRI Expert Analysis Tool) and MELODIC (Multivariate Exploratory Linear Optimized Decomposition into Independent Components) pipeline in FSL software tools (12, 13).

The processing steps included: subject motion correction using a rigid-body linear transformation from FLIRT tool [FMRIB Linear Registration Tool (14)], registering each acquired volume to the first volume; correction for temporal shift in acquisition (slice timing correction) realigned to the middle slice of each volume and high-pass temporal filter ($\sigma = 100$ s), to minimize excessive low-frequency drifts that could affect the ICA decomposition. Movements were restricted with foam padding and straps over the forehead and under the chin (estimated translation and rotation parameters were inspected and never exceeded 2 mm or 2°).

Before group ICA and the subsequent statistical analysis, for each subject a mean rs-fMRI echo-planar imaging (EPI) volume was created. All nonbrain voxels were removed and a mean EPI brain volume was extracted (15). These EPI brain mean volumes were then used to create binary brain masks, which were registered to each individual high-resolution anatomical brain volumes, using a six-degree linear transformation. Each subject's high-resolution T1-weighted structural data were brain-extracted (16) and registered to the standard stereotactic Montreal Neurological Institute (MNI) anatomical template, using 12° nonlinear transformations for optimal accuracy. Finally, the generated transformation matrix was applied to functional data to convert the rs-fMRI volumes into MNI space (17).

For ICA-based analysis, a multisubject temporal concatenation of the resting-state blood oxygen level-dependent (BOLD) signals from controls and CD patients was used according to the MELODIC pipeline (18), to find resting-state networks from multisubject rs-fMRI datasets (variance-normalized time courses). Before the ICA estimation and to avoid overfitting, the number of components from the concatenated data were calculated using Bayesian estimators and then reduced using principal components analysis. Estimated MELODIC components typically fall into two classes: those which describe effects common to all or most subjects, and those which describe effects only for a small number of subjects. The former will have a nonzero estimated effect size and the latter will have an effect size around 0 for most subjects and only few high nonzero values. The components are arranged in order of decreasing amount of median response amplitude (19).

In addition, a region of interest (ROI)-to-ROI functional connectivity analysis was performed [CONN Toolbox framework (20)]. Based on the default mode network (DMN) parietal ROIs from ICA fMRI analysis, the average temporal BOLD signal for each ROI was extracted and the functional connectivity measures between these two ROIs were obtained. ROI-to-ROI connectivity matrices were computed for each subject using bivariate correlation (Fisher *z*-transformed correlation coefficients) as a measure of "total" functional connectivity between the two ROIs. In the group analysis, all connectivity matrices from all subjects were entered into general linear model for statistics. Contrasts of interest were tested, by comparing the patterns of functional connectivity between groups. The results were thresholded at $P < 0.05$, corrected for multiple comparisons

across ROIs, using analysis-wise method to control for false positive (false discovery rate, FDR).

Choice of ROIs (Based on rs-fMRI Data). The spatial component from the estimated ICA group analysis, which describes the most common effect to all subjects (patients and controls) was selected as an a priori ROI to perform the subsequent probabilistic tractography. This selected spatial component represents the common regions found in the DMN (21). A thresholded binary mask was used to discriminate the DMN regions into specific binary mask files and the bilateral parietal components of the DMN (right and left hemisphere) were selected as ROIs for further analyses. In addition, these ROIs were then transformed into each subject's native space by applying an inverse transformation native-to-MNI matrix (or MNI-to-subject matrices). Finally, these ROIs were used as seeds for the probabilistic tractography approach.

Probabilistic Tractography. Probabilistic tractography was performed using DTIFit 2.0, FDT (FMRIB's Diffusion Toolbox, part of FSL Software Library) (22). After the fractional anisotropy (FA) maps were calculated from the eigenvalues, color-coded maps were generated from the FA values and three vector elements of v1 to visualize the white-matter tract orientation. FA images were brain-extracted (16) and registered to a common space (MNI 152), using constrained nonlinear registration [Image Registration Toolkit (23)]. Nondiffusion and diffusion images were coregistered to correct for movement artifacts and eddy current distortion effects on EPI readout. Fiber tracking, Bayesian Estimation of Diffusion Parameters Obtained using Sampling Techniques, modeling for crossing fibers (BEDPOSTX, part of FSL Software Library) was used to build up distributions of diffusion parameters at each voxel [Markov chain Monte Carlo sampling technique (24)]. The fibers estimation per voxel was then verified and, as shown in Fig. S5, the 32-diffusion direction acquisition could successfully support two fibers per voxel with good reliability.

Original individual FA maps were registered to the FA template in the MNI space (FMRIB58 FA template), using a nonlinear registration tool [FNIRT, FSL (15)]. The probabilistic tractography was performed (PROBTRACKX, FSL) in the native space of each subject (22).

To investigate the interhemispheric connectivity, a two-ROI-approach diffusion tensor imaging (DTI) probabilistic tractography was performed and the results compared among patients and controls. For the two-ROIs approach, the bilateral parietal ROIs (obtained from the DMN functional network as defined above) were used as seeds in each subject. The resulting interhemispheric fiber connectivity topography was then compared between CD subjects and controls. Next, the probabilistic streamlines between two ROIs based on the connectivity distribution values between them were computed. To directly correlate structural and functional connectivity in CD, the connectivity distribution values, obtained from probabilistic tractography, were correlated to the functional connectivity, Fisher z-transformed coefficients (Pearson correlation).

High-Angular Resolution Diffusion Imaging Processing. To best ensure that differences between groups could not be a result of missing major populations of fiber crossings, three fibers were modeled in each voxel and the automatic relevance determination parameter was set to 0.5. To visualize voxels where multiple fibers are supported, a threshold f-value of 0.05 was used. As shown in Fig. S6, the high-angular resolution diffusion imaging (HARDI) acquisition (128 diffusion-encoding directions) could successfully estimate three-way crossing fibers per voxel with good reliability.

Confirmatory analysis of interhemispheric connectivity was performed using HARDI probabilistic tractography with a two-ROI approach in two CD individuals and one control, who were rescanned. As described above, the seed ROIs were based on DMN functional parietal network of each participant. The resulting interhemispheric fiber connectivity topography was then compared between CD subjects and controls.

1. Albert M, Cohen C (1992) The Test for Severe Impairment: An instrument for the assessment of patients with severe cognitive dysfunction. *J Am Geriatr Soc* 40(5): 449–453.
2. Oldfield RC (1971) The assessment and analysis of handedness: The Edinburgh inventory. *Neuropsychologia* 9(1):97–113.
3. Brito GN, Brito LS, Paumgartten FJ, Lins MF (1989) Lateral preferences in Brazilian adults: An analysis with the Edinburgh Inventory. *Cortex* 25(3):403–415.
4. Wechsler D (1991) *Wechsler Intelligence Scale for Children (WISC-III): Manual* (The Psychological Corp., San Antonio, TX).
5. Wechler D (1997) *WAIS-III: Administration and Scoring Manual* (The Psychological Corp., San Antonio, TX).
6. Mahoney FI, Barthel DW (1965) Functional evaluation: The Barthel Index. *Md State Med J* 14:61–65.
7. Dollinger SJ, Goh DS, Cody JJ (1984) A note on the congruence of the WISC-R and the cognitive development scales of the personality inventory for children. *J Consult Clin Psychol* 52(2):315–316.
8. Silverstein AB (1985) An appraisal of three criteria for evaluating the usefulness of WAIS-R short forms. *J Clin Psychol* 41(5):676–680.
9. Welkowitz M, et al. (1991) *Introductory Statistics for the Behavioral Sciences* (Harcourt, Brace, Jovanovich, Philadelphia), 4th Ed.
10. Siegel S, Castellan NJ (1988) *Nonparametric Statistics for the Behavioural sciences* (McGraw-Hill, New York).
11. Cohen J (1992) A power primer. *Psychol Bull* 112(1):155–159.
12. Hyvärinen A (1999) Fast and robust fixed-point algorithms for independent component analysis. *IEEE Trans Neural Netw* 10(3):626–634.
13. Jenkinson M, Beckmann CF, Behrens TE, Woolrich MW, Smith SM (2012) FSL. *Neuroimage* 62(2):782–790.
14. Beckmann CF, Smith SM (2004) Probabilistic independent component analysis for functional magnetic resonance imaging. *IEEE Trans Med Imaging* 23(2):137–152.
15. Jenkinson M, Smith SM (2001) A global optimisation method for robust affine registration of brain images. *Med Image Anal* 5(2):143–156.
16. Smith SM (2002) Fast robust automated brain extraction. *Hum Brain Mapp* 17(3): 143–155.
17. Jenkinson M, Bannister P, Brady M, Smith S (2002) Improved optimization for the robust and accurate linear registration and motion correction of brain images. *Neuroimage* 17(2):825–841.
18. Tipping ME, Bishop CM (1999) Probabilistic principal component analysis. *J R Stat Soc, B* 61(Part 3):611–612.
19. Beckmann CF, Smith SM (2005) Tensorial extensions of independent component analysis for multisubject FMRI analysis. *Neuroimage* 25(1):294–311.
20. Whitfield-Gabrieli S, Nieto-Castanon A (2012) Conn: A functional connectivity toolbox for correlated and anticorrelated brain networks. *Brain Connect* 2(3):125–141.
21. Greicius MD, Supekar K, Menon V, Dougherty RF (2009) Resting-state functional connectivity reflects structural connectivity in the default mode network. *Cereb Cortex* 19(1):72–78.
22. Behrens TE, Berg HJ, Jbabdi S, Rushworth MF, Woolrich MW (2007) Probabilistic diffusion tractography with multiple fibre orientations: What can we gain? *Neuroimage* 34(1):144–155.
23. Rueckert D, et al. (1999) Nonrigid registration using free-form deformations: Application to breast MR images. *IEEE Trans Med Imaging* 18(8):712–721.
24. Behrens TEJ, et al. (2003) Characterization and propagation of uncertainty in diffusion-weighted MR imaging. *Magn Reson Med* 50(5):1077–1088.

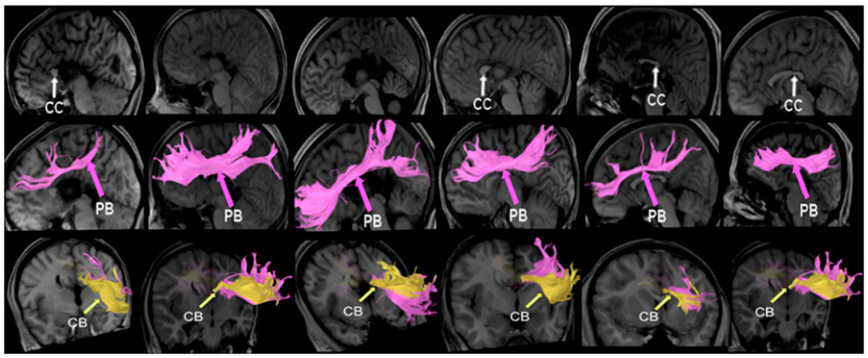

Fig. S1. The Probst bundle is found in all CD subjects. (*Top*) T1 sagittal views of six cases with different degrees of dysgenesis of the corpus callosum (CC), from agenesis to partial dysgenesis with frontal remnants and lack of the body and splenium, or a hypoplasic CC. (*Middle*) Tractography of the Probst bundles (PB, in purple) in parasagittal planes. (*Bottom*) Double documentation of Probst and cingulate bundles in coronal planes (CB, in yellow; PB, in purple), showing that both run parallel and adjacent to each other.

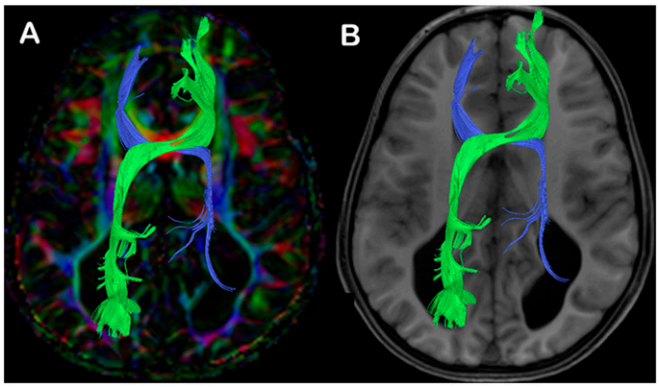

Fig. S2. The sigmoid bundles are present in some CD subjects. DTI tractography of the sigmoid bundles (in green and blue), demonstrating their usual trajectories and asymmetry. (*A*) Tractography over color-coded FA transverse plane. (*B*) Tractography over T1 transverse plane. The bundle connecting the right anterior with the left posterior areas (green) is consistently thicker than the opposite tract (blue).

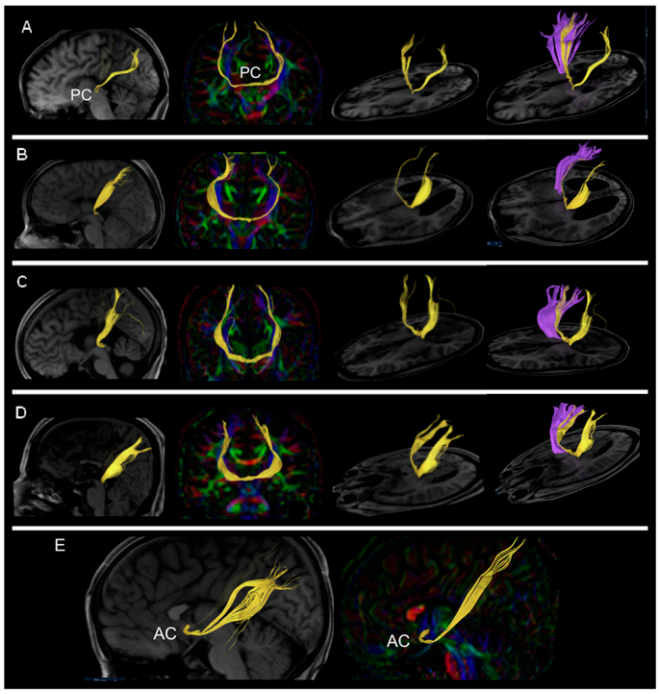

Fig. S3. Aberrant interhemispheric bundles cross at the topography of the posterior and anterior commissures. (*A*–*D*) Tractography projections on anatomical (T1-weighted MRI) sagittal/parasagittal and axial planes (first, third, and fourth columns from left), and on coronal color-coded FA maps (second column). The aberrant midbrain bundle is shown in yellow in four CD subjects, crossing at the level of the posterior commissure (PC). DTI tractography of the corticospinal tracts is displayed in purple, on the right. (*E*) Tractography projections on anatomical sagittal/parasagittal planes (T1-weighted MRI at left, color-coded FA map at right) in one subject showing the aberrant ventral forebrain bundle (in yellow) crossing through the anterior commissure (AC).

A

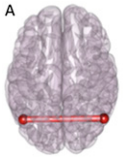

B

ROI-to-ROI	beta	t	p-FDR
CTL	1.01	11.53	0.00
CD	0.80	3.30	0.04
CD *vs.* CTL	0.21	0.81	0.67

Fig. S4. Functional connectivity in patients and controls. (*A*) Functional connectivity between left and right ROIs located at the posterior parietal cortex control (CTL) and CD groups. (*B*) There were no connectivity differences between CTL and CD. The table shows β-regression coefficients, *t* and *P* values (FDR-corrected for multiple comparisons) from the second-level general linear model analyses.

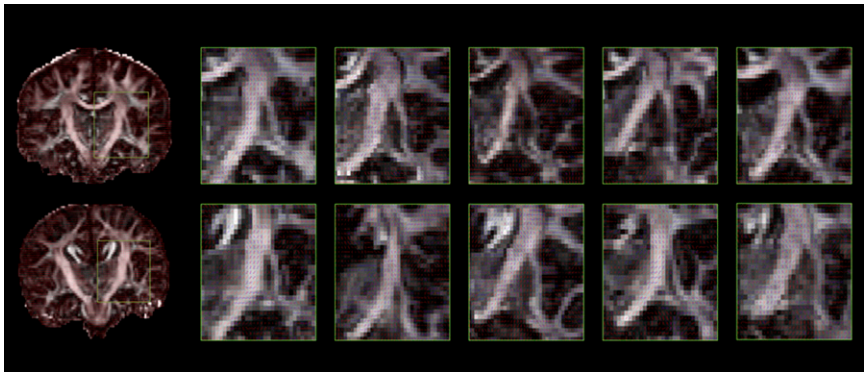

Fig. S5. Diffusion postprocessing results. *Upper* illustrates one control subject and *Lower* shows a CD subject, demonstrating that two fibers per voxel can be successfully estimated.

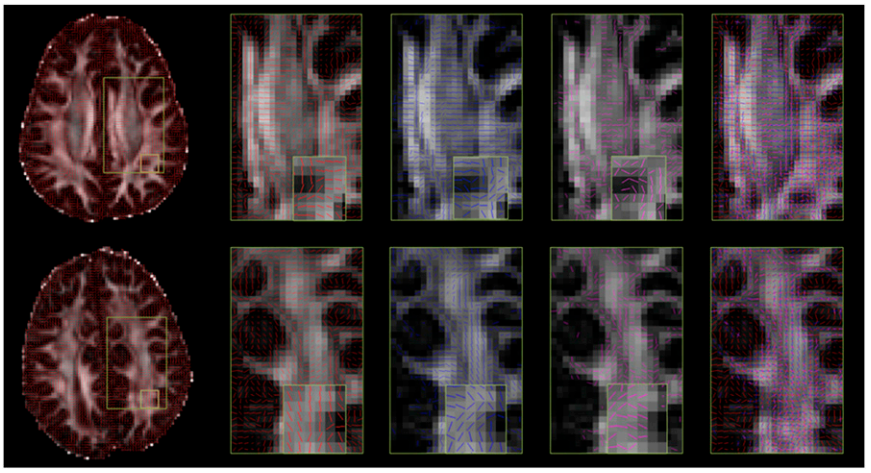

Fig. S6. HARDI postprocessing results. *Upper* shows a control subject, and *Lower* illustrates a subject with CD. It can be seen that three fibers per voxel are successfully estimated. Zoomed images are provided at the locations defined by the rectangles.

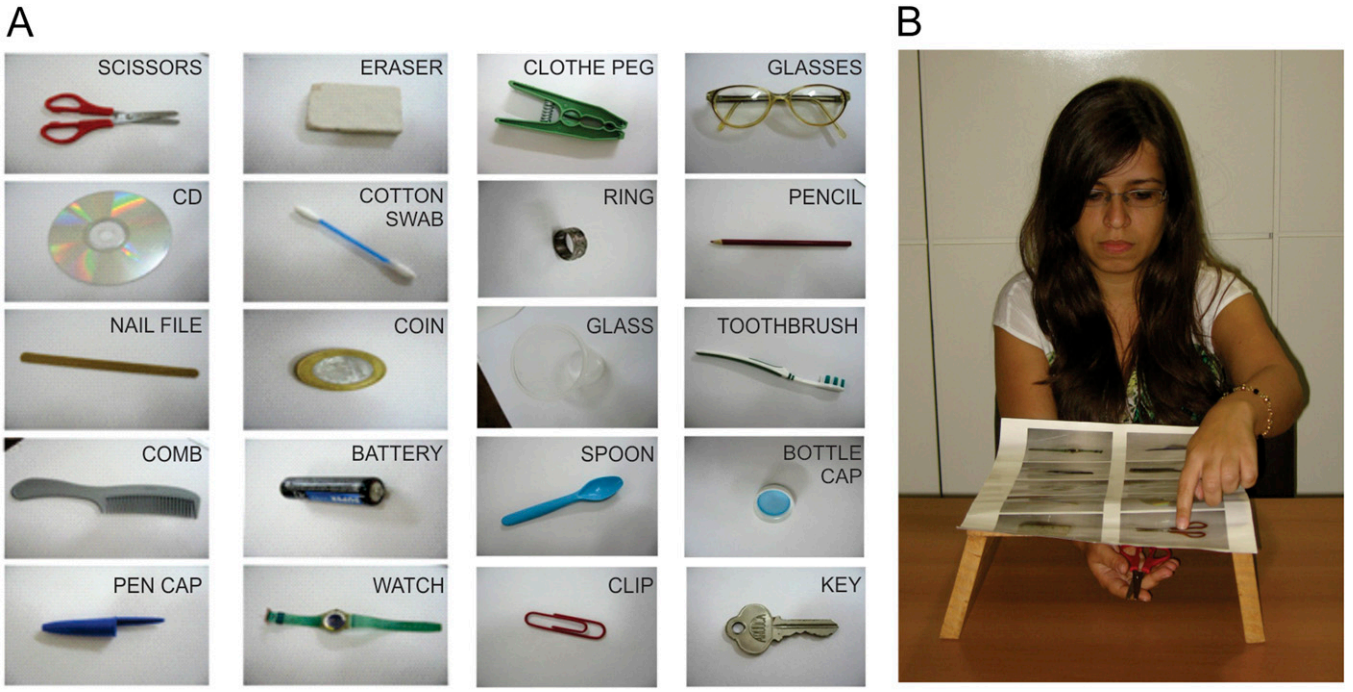

Fig. S7. Tactile and visuotactile recognition and naming tests. (*A*) Pictures of the 20 test objects. (*B*) Picture of one of the experimenters simulating the task. Note that, by design, the subject actively explores the test object with one hand, and points to the answer with the other hand.

Table S1. General summary of CD cases

Cases	CD01	CD02	CD03	CD04	CD05	CD06
Type of dysgenesis	Partial/genu remmant	Total (agenesis)	Total (agenesis)	Partial/genu remmant	Hypoplasia	Hypoplasia
Probst bundle	Present	Present	Present	Present	Present	Present
Sigmoid bundle	Present	Absent	Absent	Present	Present	Absent
Homotopic interhemispheric bundles	Midbrain	Midbrain	Midbrain	Ventral forebrain	Absent	Midbrain
DTI	Yes	Yes	Yes	Yes	Yes	Yes
HARDI	No	Yes	Yes	No	No	No
rs-fMRI	Yes	Yes	Yes	Yes	Yes	No
Neuropsychological evaluation	Yes	Yes	Yes	Yes	Yes	No

Table S2. Scores obtained by each subject on the neuropsychological inventories and tests

Tests/cases	Range	CD01	CD02	CD03	CD04	CD05
IQ	55–145*	72.5	105	90	102.5	80
Edinburgh Handedness Inventory	−100/+100	−60	100	−100	100	100
Barthel Index	0–100	80	100	90	100	90
Test for severe impairment	0–24	12	23	23	23	23
Writing R/L	0–1	—	1/1	1/1	1/1	1/1
Ideomotor praxis R/L	0–3	2/2	3/3	3/3	3/3	3/3
Tactile recogniton R/L	0–10	10/9	10/10	10/10	10/9	10/10
Tactile naming R/L	0–10	—	10/10	10/9	10/9	8/8
Visuotactile recogniton R/L	0–10	10/10	10/10	10/10	10/10	10/10
Visuotactile naming R/L	0–10	—	10/10	10/9	10/9	8/9

*±3 SD from the population mean.